Plasmonics
https://doi.org/10.1007/s11468-018-0834-z

High-Resolution Plasmonic Filter and Refractive Index Sensor Based on Perturbed Square Cavity with Slits and Orthogonal Feeding Scheme

Nikolina Janković[1] · Norbert Cselyuszka[1]

Received: 26 April 2018 / Accepted: 20 August 2018

Abstract
We present a plasmonic bandpass filter and refractive index sensor based on perturbed square cavity resonator with slits, which is fed by orthogonally oriented feeding waveguides. The slits provide size reduction in comparison to conventional square cavities and better coupling to the waveguides, while the perturbation and orthogonal feeding scheme provide a pair of transmission zeros in the response of the structure. In that manner, a bandpass filter with high transmission, narrow bandwidth, and excellent selectivity can be readily designed. Moreover, with a slight modification of the structure, a very sharp Fano-like response can be obtained and employed for refractive index sensing with high sensitivity and figure of merit.

Keywords Plasmonics · Cavity resonator · Bandpass filter · Refractive index sensor

Fast development of optical communication systems constantly imposes high demands in terms of transmission speed, capacity, cost, and compactness. In such systems, employment of conventional optical elements is very disadvantageous because of their large size, which is of the order of wavelength. Due to specific nature and ability to overcome diffraction limit, surface plasmon polaritons (SPP) and plasmonic components represent a very promising alternative [1–3]. One of the SPP guiding structures are metal-insulator-metal (MIM) slabs, which are very suitable for highly integrated photonic circuits and they offer a very good trade-off between light confinement and energy loss [4]. Therefore, various components based on MIM waveguides have been proposed including filters [5–14], splitters [15], demultiplexers [16], power dividers [17], and sensors [18–26].

When it comes to filters, which are of crucial importance in optical systems, there have been proposed different plasmonic configurations to achieve filtering operation, such as circular [12], square [8, 11], and rectangular cavities [13], as well as stub [5], ring [6, 9, 10], spiral [7], and complementary split ring resonators [14]. However, most filters cannot simultaneously meet the requirements for a very accurate wavelength selection, low loss, and compactness. Moreover, rarely do filters exhibit multiple transmission zeros in their response which further limit the possibility for high-filtering resolution.

In this paper, we present a plasmonic bandpass filter based on a perturbed square cavity with slits fed by orthogonally oriented waveguides. In that manner, significant compactness is achieved, together with high-transmission level, narrow bandwidth, and excellent selectivity. With a slight modification of the structure, a very sharp fano-like response can be obtained and employed for refractive index sensing with high sensitivity and figure of merit.

The layout of the structure and the corresponding geometrical parameters are shown in Fig. 1. It consists of a square cavity resonator with symmetrically positioned rectangular slits, and small square perturbation positioned at the upper right corner, while the feeding MIM waveguides are mutually orthogonally oriented. The white area represents air whose refractive index is equal to 1, while the blue area represents silver which is characterized using Drude model [27]:

$$\varepsilon_m = \varepsilon_\infty - \frac{\omega_p^2}{\omega^2 + i\omega\gamma} \tag{1}$$

where the permittivity at the infinite frequency ε_∞ is equal to 3.7, plasma frequency ω_p is 1.38 10^{16} rad/s, and the damping frequency γ equals 2.73 10^{13} Hz. The width of the MIM waveguides w has been chosen to be 50 nm to provide that only the fundamental transverse magnetic (TM0) mode is supported, while the length of the square cavity L has been

✉ Norbert Cselyuszka
cselyu@biosense.rs

[1] BioSense Institute-Research and Development Institute for Information Technologies in Biosystems, University of Novi Sad, Novi Sad, Serbia

Published online: 30 August 2018

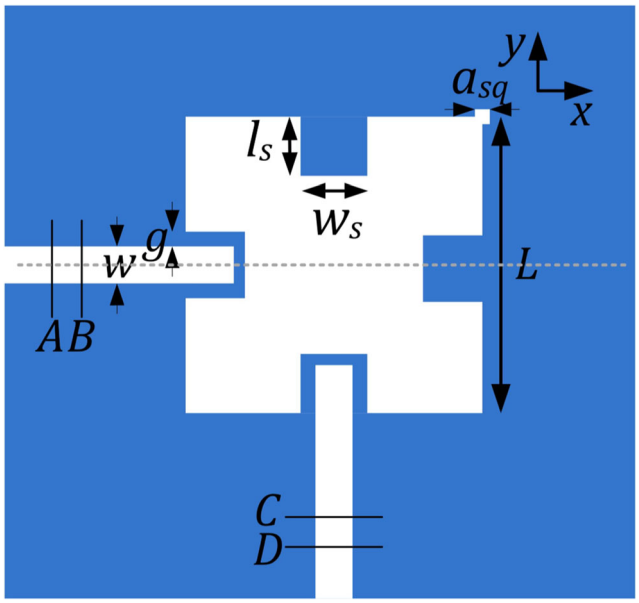

Fig. 1 Configuration of the proposed structure

set to 400 nm and width of the slits w_s 90 nm.

The role of the rectangular slits is twofold—they provide size reduction in comparison to the conventional square cavity resonator and they can accommodate the waveguides so better coupling between the waveguides and resonator can be achieved as well as higher transmission level. Fig. 2a shows how the spectral position of the two fundamental degenerative modes, TM_{10} and TM_{01}, changes with the length of the slits. To that end, Comsol Multiphysics solver and eigenmode analysis have been used. It can be seen that the increase of the l_s can significantly reduce the fundamental resonant wavelength. However, the length of the slits should not be excessively increased, since the cavity nature of the resonator and consequently good quality factor would be lost. Therefore, l_s has been set to 80 nm.

To achieve a high-performance, narrowband, and highly selective filtering operation, it is desirable to have more than one pole in the response, i.e., to include more than one resonance. At the same time, the poles should be closely positioned in the spectrum and transmission zeros that are closely positioned to the passband should be provided.

To that end, in the proposed configuration, the feeding waveguides are orthogonally oriented, and a small square perturbation is positioned at the upper right corner of the square cavity. As stated previously, the two fundamental modes TM_{10} and TM_{01} are degenerative modes and have orthogonal field distribution and the same resonant frequency, Fig. 2. To employ them as two closely positioned poles in the filter, the square perturbation is introduced in the structure. Fig. 3a shows how the resonant wavelengths of the modes are changed with the parameter a_{sq}, while Fig. 3b, c shows how the field distribution in the square cavity is changed once the perturbation is introduced.

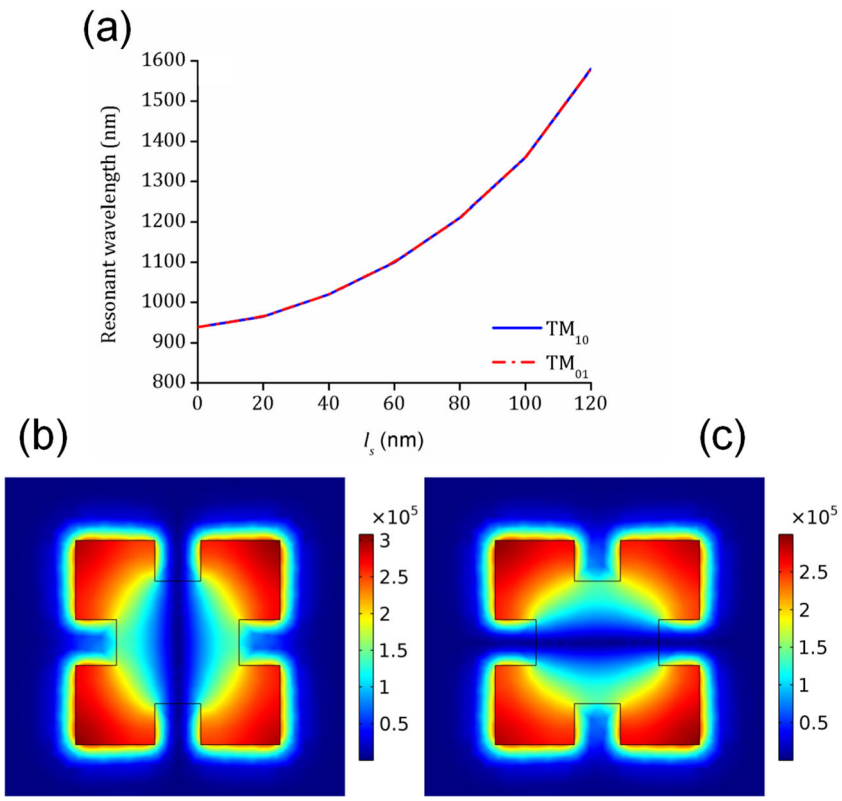

Fig. 2 **a** Change of the resonant wavelength of TM10 and TM01 modes with the parameter *ls* for the structure with no perturbation. **b** Normalized Hz field distribution of TM10 mode. **c** Normalized Hz field distribution of TM01 mode

Higher values of the parameter a_{sq} causes the higher difference in the resonant wavelength of the fundamental modes, i.e., more pronounced blueshift of one of the fundamental modes, Fig. 3a. At the same time, the other fundamental mode remains unchanged, due to the fact that the perturbation is positioned at the corner at which the magnetic field of one mode exhibits peak, and the magnetic field of the other mode exhibits zero and thus it is not influenced by the perturbation.

The perturbation somewhat rotates the original fields, and the field poles and zeros are located at the corners of the square cavity. Consequently, the proposed feeding scheme allows that the two modes are simultaneously excited, which would not be possible in the configuration without perturbation. Moreover, each waveguide feeds the cavity in the manner that it is simultaneously coupled to the points of strong and weak magnetic fields of the modes. Intuitively, this can be understood that the modes are simultaneously strongly and weakly excited, and consequently transmission peaks and transmission dips can occur very closely in the spectrum.

Based on the previous analysis and the optimization of the parameters, a bandpass filter has been designed and the final values of the geometrical parameters are: $L = 400$ nm, $l_s = 80$ nm, $w_s = 90$ nm, $w = 50$ nm, $g = 20$ nm, and $a_{sq} = 20$ nm.

The transmission response obtained in Comsol Multiphysics is shown in Fig. 4. To find the scattering matrix for the proposed structure four planes were defined (A, B, C, D) as it is shown in Fig. 1. The distance between A and B and C and D is equal to 50 nm, while the distance between B and the filter and between C and the filter is 400 nm. In these four planes, the magnetic field H_z in complex form was determined, and using those values the reflected and transmitted wave components can be separated, and the elements of the scattering matrix calculated [28]. Since the system is a symmetrical and reciprocal, $S_{11} = S_{22}$ and $S_{12} = S_{21}$. The transmission coefficient T and the reflection coefficient R can be calculated as $T = |S_{21}|^2$ and $R = |S_{11}|^2$, respectively.

The central wavelength of the passband is 1228 nm, and the passband is characterized by good transmission level. Excellent selectivity and narrow bandwidth are provided by two transmission zeros that are symmetrically positioned around the passband at 1171 and 1285 nm. Full width at half maximum (FWHM) is only 23 nm, i.e., 1.87%, which confirms very narrow bandwidth not readily obtained in other plasmonic filters.

The proposed configuration can be also analyzed using temporal-coupled mode theory (CMT) using the following expressions [29]:

$$\frac{da_1}{dt} = \left(j\omega_1 - \frac{1}{\tau_{10}} - \frac{1}{\tau_{11}} - \frac{1}{\tau_{12}}\right)a_1 + \kappa_{11}s_{1+} + \kappa_{12}s_{2+} - j\mu a_2, \tag{2}$$

$$\frac{da_2}{dt} = \left(j\omega_2 - \frac{1}{\tau_{20}} - \frac{1}{\tau_{21}} - \frac{1}{\tau_{22}}\right)a_2 + \kappa_{21}s_{1+} + \kappa_{22}s_{2+} - j\mu a_1, \tag{3}$$

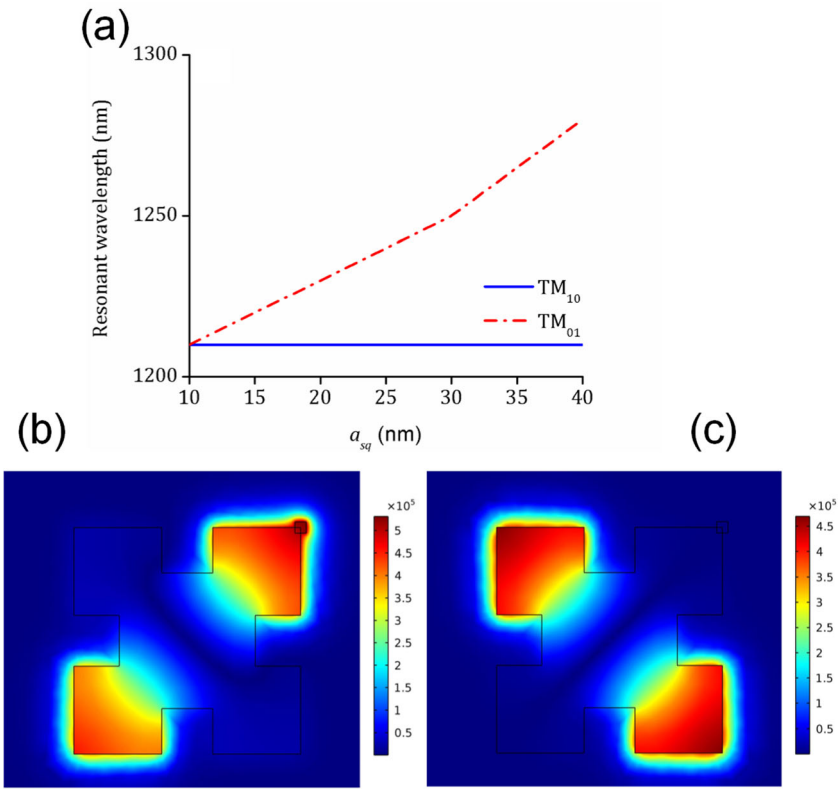

Fig. 3 **a** Change of the resonant wavelength of TM_{10} and TM_{01} modes with the parameter a_{sq} for the structure with perturbation. **b** Normalized H_z field distribution of TM_{10} mode. **c** Normalized H_z field distribution of TM_{01} mode

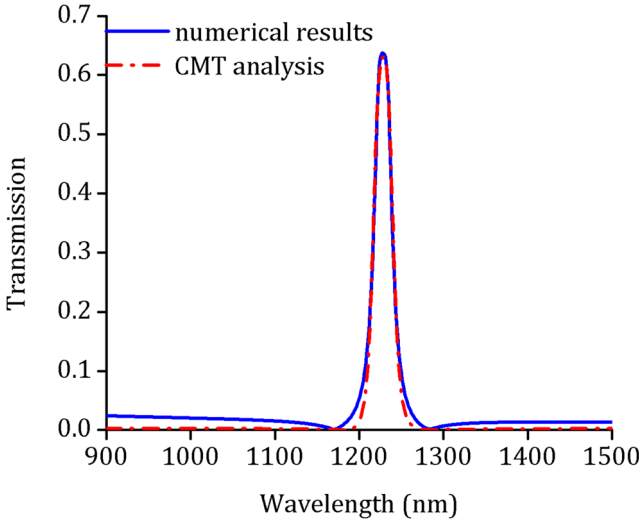

Fig. 4 Comparison of transmission response of the filter obtained numerically and using CMT analysis

$$s_{(1-)} = -s_{(1+)} + \kappa_{11}^{*} a_1 + \kappa_{21}^{*} a_2 + j\kappa_w s_{2+}, \tag{4}$$

$$s_{2-} = -s_{2+} + \kappa_{12}^{*} a_1 + \kappa_{22}^{*} a_2 + j\kappa_w s_{1+}, \tag{5}$$

$$\kappa_{11} = \sqrt{\frac{1}{\tau_{11}}} e^{j\theta_{11}}, \kappa_{12} = \sqrt{\frac{1}{\tau_{12}}} e^{j\theta_{12}}, \kappa_{21} = \sqrt{\frac{1}{\tau_{21}}} e^{j\theta_{21}}, \kappa_{22} = \sqrt{\frac{1}{\tau_{22}}} e^{j\theta_{22}}, \kappa_w = \sqrt{\frac{1}{\tau_w}} e^{j\theta_w}, \tag{6}$$

where a_1 and a_2 represent the resonant modes, ω_1 and ω_2 their resonant frequencies, and τ_{10} and τ_{20} decay times of their internal loss. The parameters τ_{11}, τ_{12}, τ_{21}, and τ_{22}, are decay times of the coupling between the resonant modes and waveguides, and θ_{11}, θ_{12}, θ_{21}, and θ_{22}, are the corresponding coupling phases, while $s_{i\pm}$ are the field amplitudes in each waveguide ($i = 1, 2$, for outgoing (−) or incoming (+) from the resonator). The coefficient κ_w stands for the coupling between the waveguides, while the coupling coefficient between the two cavity modes is denoted by μ. Namely, according to the field distribution, it can be considered that both modes are coupled to both feeding waveguides, which is expressed through the second and third terms in Eqs. (4) and (5). The fourth term in the same expressions indicates that the two waveguides are mutually coupled, and although the coupling is very weak, it contributes to the existence of the pair of symmetrically positioned transmission zeros [30].

Since s_{2+} can be considered zero, the transmission response can be expressed as follows:

$$T = |t|^2 = \left| \frac{\kappa_{12}^{*}\left(\kappa_{21} - \frac{\kappa_{11}}{j\mu(j(\omega-\omega_2)+N)}\right) + \kappa_{22}^{*}\left(\kappa_{11} - \frac{\kappa_{21}}{j\mu(j(\omega-\omega_1)+M)}\right)}{j\mu + \frac{1}{\mu}(j(\omega-\omega_1)(\omega-\omega_2) + N(\omega-\omega_1) + M(\omega-\omega_2) - jMN)} + \kappa_w \right|^2 \tag{7}$$

$$M = \frac{1}{\tau_{10}} + \frac{1}{\tau_{11}} + \frac{1}{\tau_{12}}, N = \frac{1}{\tau_{20}} + \frac{1}{\tau_{21}} + \frac{1}{\tau_{22}}. \tag{8}$$

The resonant frequencies ω_1 *and* ω_2 and the internal decay times have been determined using eigenmode analysis in Comsol Multiphysics solver and the following expression $\tau_{n0} = 2Re(\omega_i)/(2\omega_i Im(\omega_i))$, where $i = 1, 2$. The coupling factor μ has been approximated as $\mu = \omega_2/(2(\omega_2 - \omega_1))$ [31]. The decay times between the resonant modes and waveguides have been approximated as $\omega_2/\delta\omega$, where $\delta\omega$ is the width of the frequency range in which the S_{11} phase changes the phase from $-\pi/2$ to $\pi/2$. After the optimization and fitting of the CMT model response to the numerical one, the following values of the parameters have been obtained: $\omega_1 = 2\pi\ 2.44\ 10^{15}$ rad/s, $\omega_2 = 2\pi\ 2.47\ 10^{15}$ rad/s, $\tau_{10} = 356$ fs, $\tau_{20} = 363$ fs, $\tau_{11} = 120$ fs, $\tau_{12} = 650$ fs, $\tau_{21} = 650$ fs, $\tau_{22} = 120$ fs, $\tau_{22} = 120$ fs, $\tau_w = 700$ s, $\theta_{11} = 0.1\pi$, $\theta_{12} = -0.55\pi$, $\theta_{21} = 0.25\pi$, $\theta_{22} = 0.6\pi$, $\theta_w = 1.1\pi$, and $\mu = 1.15\ 10^{13}$.

Figure 4 shows the comparison between the numerically obtained response and the fitted one and an excellent agreement can be observed.

Since the proposed structure exhibits the narrowband response and transmission zeros, it can be intuitively understood that with slight modifications in the structure, a sharp fano-like response can be obtained, which can be used for the sensing purposes. To that end, the structure without the square perturbation has been investigated. Figure 5 shows that in this case a response with one transmission pole and a pair of asymmetrically positioned transmission zeros can be obtained, where one of the zeros forms a very steep peak-to-dip slope. Namely, Fig. 5 shows how the response is changed when the symmetry axis of the first waveguide (with *A* and *B* planes) and the corresponding slit is moved away from the axis shown in the gray dotted line in Fig. 1, while the other parameters remain the same. For the deviation from the gray axis d = 20 nm a good trade-off between the transmission level and peak-to-dip slope is obtained, 0.61 and 30 nm, respectively,

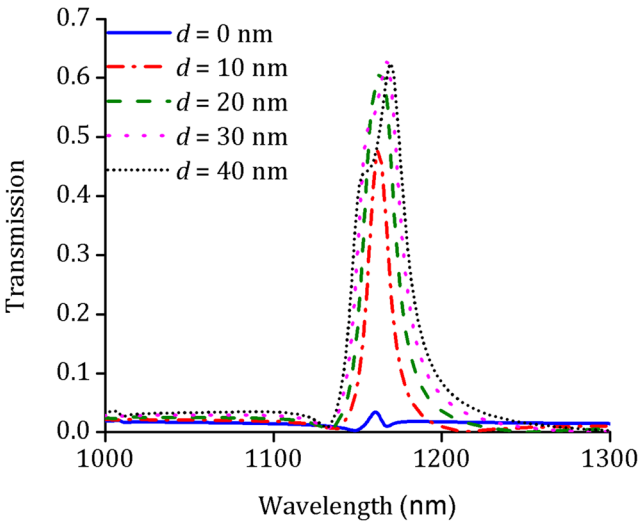

Fig. 5 Response of the square cavity without perturbation for different values of d

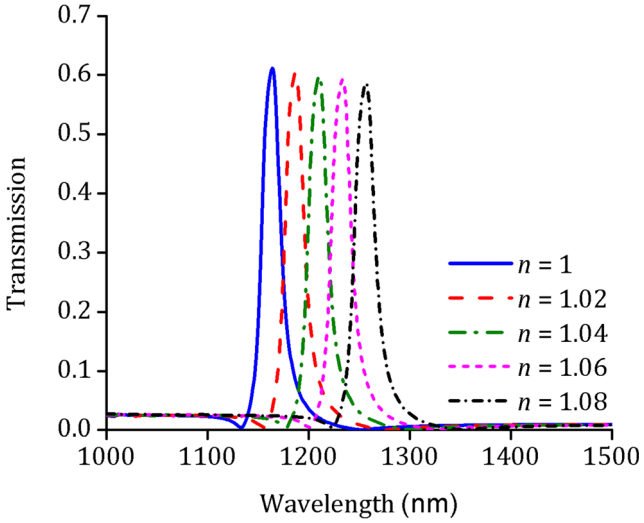

Fig. 6 Responses of the sensor for different refractive indices

and this structure has been further investigated for the sensing purposes. We note here that in the sensing structure the parameter l_s is equal to 70 nm, which causes a slight blueshift if the response, whilst the other parameters remain the same as in the case of the filter.

Sensing potential of the structure is demonstrated through its response for different refractive indices of the dielectric marked in white in Fig. 1. The refractive index has been varied from 1 to 1.08 with the step of 0.02 and the corresponding responses are shown in Fig. 6. The sensitivity of a sensor (nm/RIU) is usually defined as the shift in the resonance wavelength per unit variations of the refractive index [24]. According to the responses, the sensitivity is equal to 1150 nm/RIU.

Another important and more illustrative parameter of a sensor performance is figure of merit (FOM), which is defined

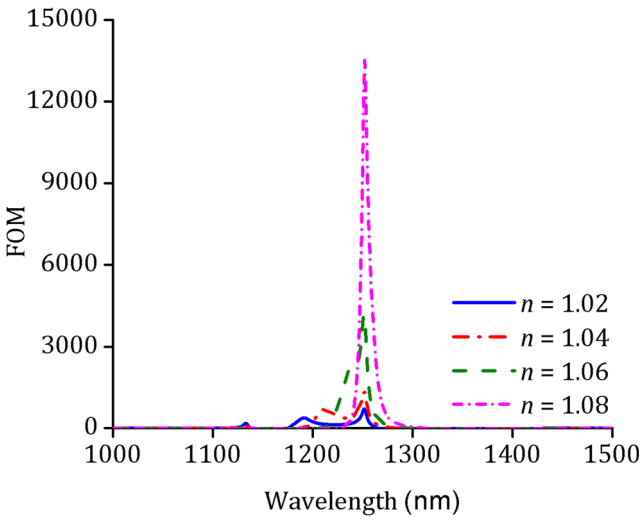

Fig. 7 Calculated FOM for different refractive indices

Table 1 Comparison of the proposed sensor and other recently published similar solutions

Reference	Sensitivity [nm/RIU]	FOM
[18]	1200	200
[20]	100	840
[21]	1090	33,340
[22]	1900	38,000
[23]	3476	124.6
[24]	938	13,500
[25]	1562.5	NA
[26]	NA	900
This work	1150	13,500

as FOM = $\Delta T/T\Delta n$ [24]. T denotes the transmittance in the proposed structure and $\Delta T/\Delta n$ denotes the transmission change at the fixed wavelength induced by a refractive index change. Fig. 7 shows FOMs calculated for the refractive index 1.02, 1.04, 1.06, and 1.08 as FOM = $(T_{n\ =1.02/1.04/1.06/1.08} - T_{n\ =1})/(T_{n\ =1}\Delta n)$. Although the curves differ in the maximal values, it can be considered that FOM can reach the values of the order of 10^3–10^4.

In Table 1, the sensitivity and FOM of different structures are compared to those of the proposed structure. As it can be seen, the proposed structure has comparable or higher FOM than the other structures, except for [21, 22]. As for the sensitivity, only the structures in [22, 23] exhibit significantly better sensitivity. However, high FOM and sensitivity in the structure in [22] is achieved at the expense of the low-transmission level, while the structure in [23] exhibits very low FOM. Moreover, we note again that the proposed structure has a twofold purpose which represents its particular strength. Besides operating as a filter, the proposed structure can also be readily transformed to a sensor with excellent performance, which is not the case with other sensors.

To conclude, we proposed a novel plasmonic structure based on perturbed square cavity resonator with slits, which has a great potential for applications in filtering operation and sensing. A small square perturbation introduced in the structure and the orthogonal feeding scheme provides two-pole, narrowband, and highly selective bandpass response which makes the proposed structure one of the most compact filter with excellent performance and FWHM of only 1.87%. A slight modification of the proposed structure allows for fano-like response with a very steep peak-to-dip slope, which can be readily applied in sensing. Sensing potential has been demonstrated through the response for different refractive indices of the dielectric. Sensitivity of 1150 nm/RIU and FOM of the order 10^3–10^4 have been achieved, which is comparable to the state-of-the-art solutions, and thus the proposed structure can be considered as a good candidate for sensing applications.

References

1. Maier SA (2007) Plasmonics: fundamentals and applications. Springer, Berlin
2. Barnes W, Dereux A, Ebbesen TW (2003) Surface plasmon subwavelength optics. Nature 424:824–830
3. Zayats A, Smolyaninov I, Maradudin A (2005) Nano-optics of surface plasmon polaritons. Phys Rep 408:131–314
4. Fang Y, Sun M (2015) Nanoplasmonic waveguides: towards applications in integrated nanophotonic circuits. Light Sci Appl 4:294
5. Zhang RB, Gu X, Jin X, Zhang YQ, Lee Y (2017) Unidirectional reflectionless propagation in plasmonic waveguide system based on phase coupling between two stub resonators. Photonics J IEEE 9:1
6. Wen K, Hu Y, Chen L, Zhou J, He M, Lei L, Wu Y, Li J (2017) Single- and dual-plasmonic induced absorption in a subwavelength end-coupled composite-square cavity. Appl Opt 56:8372–8377
7. Feng Y, Liu Y, Wang X, Dong D, Shi Y, Hua S, Zhang H, Tang L (2016) Compact nanofilters based on plasmonics waveguide with Archimedes' spiral nanostructure. IEEE Photon J 8:1
8. Wu W, Yang J, Zhang J, Huang J, Chen D, Wang H (2016) Ultra-high resolution filter and optical field modulator based on a surface plasmon polariton. Opt Lett 41:2310–2313
9. Wang S, Li Y, Xu Q, Li S (2016) A MIM filter based on a side-coupled crossbeam square-ring resonator. Plasmonics 11:1291–1296
10. Chang Y, Chen CH (2014) Broadband plasmonic bandstop filters with a single rectangular ring resonator. IEEE Photon Technol Lett 26:1960–1963
11. Rahimzadegan A, Granpayeh N, Hosseini SP (2014) Improved plasmonic filter, ultra-compact demultiplexer, and splitter. J Opt Soc Korea 18:261–273
12. Zhan G, Liang R, Liang H, Luo J, Zhao R (2014) Asymmetric band-pass plasmonic nanodisk filter with mode inhibition and spectrally splitting capabilities. Opt Express 22:9912–9919
13. Zhou X, Zhou L (2013) Analysis of subwavelength bandpass plasmonic filters based on single and coupled slot nanocavities. Appl Opt 52:480–488
14. Zand A, Mahigir A, Pakizeh T, Abrishamian MS (2012) Selective-mode optical nanofilters based on plasmonic complementary split-ring resonators. Opt Express 20:7516–7525
15. Guo Y, Yan L, Pan W, Luo B, Wen K, Guo Z, Li H, Luo X (2011) A plasmonic splitter based on slot cavity. Opt Express 19:13831–13838
16. Geng X, Wang T, Yang D, He L, Wang C (2016) Tunable plasmonic wavelength demultiplexing device using coupled resonator system. Photonics J IEEE 8:1
17. Dolatabady A, Granpayeh N (2015) L-shaped filter, mode separator and power divider based on plasmonic waveguides with nanocavity resonators. IET Optoelectron 9:289–293
18. Fu H, Li S, Wang Y, Song G, Zhang P, Wang L, Yu L (2018) Independently tunable ultrasharp double fano resonances in coupled plasmonic resonator system. IEEE Photon J 10(1):1–9
19. Gao Y, Wang T, Cao C, Wang C (2017) Gap induced mode evolution under the asymmetric structure in a plasmonic resonator system. Photon Res 5:113
20. Li S, Wang Y, Jiao R, Wang L, Duan G, Yu L (2017) Fano resonances based on multimode and degenerate mode interference in plasmonic resonator system. Opt Express 25:3525–3533
21. Li H, Li L, Zeng S, Zhan Z, He ZC, Xu H (2016) Sensing application in fano resonance with T-shape structure. J Lightwave Technol 34:3342–3347
22. Zhang Y, Li S, Chen Z, Jiang P, Jiao R, Zhang Y, Wang L, Yu L (2017) Ultra-high sensitivity plasmonic nanosensor based on multiple fano resonance in the MDM side-coupled cavities. Plasmonics 12:1099–1105
23. Chen L, Liu Y, Yu Z, Wu D, Ma R, Zhang Y, Ye H (2016) Numerical analysis of a near-infrared plasmonic refractive index sensor with high figure of merit based on a fillet cavity. Opt Express 24:9975–9983
24. Binfeng Y, Hu G, Zhang R, Yiping C (2016) Fano resonances in a plasmonic waveguide system composed of stub coupled with a square cavity resonator. J Opt 18:055002
25. Xie YY, Huang YX, Zhao WL, Xu WH, He C (2015) A novel plasmonic sensor based on metal–insulator–metal waveguide with side-coupled hexagonal cavity. Photonics J IEEE 7:1
26. Qi J, Chen Z, Chen J, Li Y, Qiang W, Xu J, Sun Q (2014) Independently tunable double fano resonances in asymmetric MIM waveguide structure. Opt Express 22:14688–14695
27. Wang H, Yang J, Zhang J, Huang J, Wu W, Chen D, Xiao G (2016) Tunable band-stop plasmonic waveguide filter with symmetrical multiple-teeth-shaped structure. Opt Lett 41:1233–1236
28. Åbom M (1991) Measurement of the scattering-matrix of acoustical two-ports. Mech Syst Signal Process 5:89–104
29. Haus HA (1984) Waves and fields in optoelectronics. Prentice-Hall, Upper Saddle River
30. Yu F, Wang Y, Wang Z, Zheng Q, Zhou M, Guo D, Ding X, Xu X, Wang L, Chen H, Shang Y, Huang Z (2015) Temporal coupled-mode theory and the combined effect of dual orthogonal resonant modes in microstrip bandpass filters. IEEE Trans Microw Theory Tech 63:403–413
31. Li Q, Wang T, Su Y, Yan M, Qiu M (2010) Coupled mode theory analysis of mode-splitting in coupled cavity system. Opt Express 18:8367–8382